JOURNAL OF MATERIALS SCIENCE 32 (1997) 5257–5269

Study of the sintering properties of plasma synthesized ultrafine SiC powders

J. Y. GUO, F. GITZHOFER, M. I. BOULOS
CRTP, Department of Chemical Engineering, Faculty of Applied Sciences, University of Sherbrooke, Quebec, Canada J1K 2R1

T. ISHIGAKI, M. MIENO
Research Center for Advanced Materials, National Institute for Research in Inorganic Materials, 1-1, Namiki, Tsukuba, Ibaraki 305, Japan

A study on the sintering of ultrafine SiC powders synthesized from elemental Si and CH_4 using radio frequency (r.f.) induction plasma technology is reported. The powder had a particle size in the range of 40 to 80 nm and was composed of a mixture of α and β-SiC. It was subjected to pressureless sintering in an induction furnace in the presence of different sintering aids. With the addition of B_4C (2.0 wt % B) by mechanical mixing, the powders could only be partially densified, with the highest value of 84.5% of theoretical density being achieved at 2170 °C for 30 min. Through the use of ''in-flight'' boron doping of the powder during the plasma synthesis step (1.65 wt % B), the ultrafine powder obtained could be densified to above 90% of its theoretical density at 2050 °C for 30 min. The addition of oxide sintering aids (7.0 wt % Al_2O_3 + 3.0 wt % Y_2O_3) by mechanical mixing produced sintered pellets of 95% of theoretical density at 2000 °C for 75 min. The Vicker's microhardness of the sintered pellets in this case was as high as 31.2 GPa.

In order to improve our understanding of the basic phenomena involved, extensive microstructural (scanning electron energy microscopy: SEM), physical (shrinkage, weight loss, porosity, hardness) as well as chemical analysis (prompt gamma neutron activation analysis (PGNAA), energy dispersive spectroscopy (EDS), X-ray photoelectron spectroscopy (XPS), thermogravimetric analysis (TGA)) was carried out. This helped establish a relationship between the properties of the as-synthesized powder and their sintering properties. The influences of sintering temperature, sintering time, additive concentration, and powder purity on the densification behaviour of the plasma-synthesized powders was investigated. The results were compared with data obtained using commercial powder.

1. Introduction

A number of studies have been reported on the plasma synthesis of ultrafine powder (UFP) of SiC. These used a wide range of reaction routes such as $SiH_4 + CH_4$ [1–2], $SiCl_4 + CH_4$ [3–6], CH_3SiCl_3 or $Si(CH_3)_4$ [7–10], and $SiO_2 + CH_4$ [11–12]. In a previous study [13] results were reported on the plasma synthesis of SiC UFP through the direct carburization of Si with CH_4 in an induction plasma reactor. The synthesis steps involved are: (1) vaporization of Si powder; (2) vapour phase carburization and condensation of SiC UFP. The results showed that the average particle size of the plasma synthesized powders was 40–80 nm and the specific surface areas was 25–60 $m^2 g^{-1}$. The morphology of these powders tends to be equiaxed and spherical. The powder was composed of a mixture of $\approx$ 40 wt % α-SiC and 60 wt % of β-SiC and the following impurities of varying amounts: free C 0.5–5.0 wt %, free Si 0.2–3.0 wt %, and undetected oxygen and metallic elements Al, Fe, Ca, Cu etc. which originated from source materials.

For covalently bonded compounds such as Si_3N_4 and SiC, pressureless sintering requires the use of sintering aids. Boron and carbon [14–17], or aluminium and carbon [18–19], or even boron, aluminium and carbon [20–22] as well as alumina and yttria [23–25] are some of the effective additives for the sintering of SiC powder. It is believed that SiC parts sintered with B addition retain their high temperature strength, especially their high-temperature creep resistance. Previously, directly boron doped SiC UFP have been prepared from various gas phase reaction systems, by using either plasma or laser techniques. Such reaction systems included: $SiH_4 + CH_4 + B_2H_6$ [26], $SiCl_4 + CH_4 + BCl_3$ [27] or $SiCl_4 + H_xC_yCl_z + BCl_3$ [4] in d.c. plasma, $SiH_4 + C_2H_4$ + diborane [28] in laser processing. However, reports have not been found on the synthesis and sintering of boron-doped SiC UFP from solid precursors. Additionally, submicron SiC powders, synthesized from solid precursors such as SiO_2 and Si, display only minor densification when sintered with the additions of boron and carbon [14, 29].

0022–2461

The objective of the present study is: (1) evaluation of the sintering properties of plasma synthesized UFP of SiC using different sintering aids; (2) comparison of the results with those obtained using commercially available powder; and (3) study of the *in-situ* (in-flight) doping of the SiC during the plasma synthesis step and its effect on the sintering properties of the powder obtained.

2. Sintering procedure

2.1. Powder preparation

The as-synthesized powders were stored in air for comparison with commercial powders. The SiC UFP was first sintered with the addition of B_4C and the combination of Al_2O_3 and Y_2O_3, respectively. *In situ* boron-doped SiC UFP was sintered subsequently for the comparison purpose with the B-admixed SiC UFP. The boron carbide employed was a product of Fisher Laboratory Chemical (0.75 μm by Brunauer–Emmett–Teller analysis (BET); alumina was obtained from Alcoa (0.13 μm); yttria from Hermann C. Stark (0.1 μm). The *in situ* boron-doped SiC UFP refers to the powder in which boron was incorporated during plasma synthesis, using BCl_3 as the boron source. The α-SiC powder used in this study was the commercial product available from Onoda as OY15A (average particle size: 0.16 μm).

The characteristics of the powders used in this study along with those of the additives are summarized in Table I.

The as-synthesized SiC UFP, together with the additives, were wet-mixed in *n*-hexane contained in a nylon vessel by rolling on a roll mixer apparatus for 10 h. Some small nylon beads were used as mixing aid media. The powder mixture was then dried in a vacuum oven at 80 °C for at least 5 h. The dried powders were crushed and ground in an agate mortar.

2.2. Cold pressing

A quantity of 0.3 to 0.5 g of the powder was uniaxially pressed in a ϕ10 mm tungsten carbide die under a pressure of 150 MPa. This treatment was followed by cold isostatic pressing under ~400 MPa hydrostatic pressure, using evacuated rubber bags to obtain pellets (3.5–4.0 mm in height and ~9.5 mm in diameter) with a green density of near 50% theoretical. The theoretical density was estimated on the basis of the rule of mixtures. The as-synthesized boron-doped SiC UFP was directly pressed in the tungsten carbide die and then under the cold isostatic pressing.

2.3. Pressureless sintering

Sintering was performed in an induction furnace where a graphite crucible served as the susceptor. A hole through the cover allowed us to measure the temperature pyrometrically directly on the surface of the sample. The pyrometer was calibrated in advance of sintering. Due to the generation of volatile components during firing, the temperature reading could change singificantly. In this case, the temperature was held constant by fixing plate power level at the beginning of soaking. Samples were heated to the desired soaking temperatures at a fast rate that ranged from 100 to 500 °C min^{-1}. The heating and soaking at sintering temperatures took place in an atmosphere of flowing argon. After soaking, the samples were cooled in the furnace. Fig. 1 shows a schematic of the induction sintering furnace.

3. Characterization of sintered pellets

Linear shrinkage and weight loss of its pellets after sintering were determined. The sintered pellets were ground to remove the as-sintered surface for density measurements, using the water immersion technique. Prompt gamma neutron activation analysis (PGNAA) was used to determine the boron contents in the boron-doped samples. X-ray photoelectron spectroscopy (XPS or ESCA) combined with electron probe microanalysis (EPMA) using an ultrathin Al window, was employed to analyse the compositions

TABLE I Characterization of starting materials

Sample No.	Substance	Original powder composition (wt %)				Additive concentration (wt %)
		SiC	Si_f	C_f	B	
P-BC1	Plasma powder	91.51	0.17	8.32	–	0.5; 2.0; 5.0; 10.0B
P-BC2	(mixed with B_4C)	93.77	0.23	6.00	–	0.5B
PH-B0		99.31	0.19	0.50	0.0	
PH-B1	Plasma powder	93.55	0.14	5.68	0.63	
PH-B2	(*in situ* B-doped)	92.72	0.18	5.45	1.65	
PH-B3		91.80	0.20	4.10	3.90	
P-YA1		96.71	3.05	0.24	–	5.0; 10.0; 15.0; 25.0
P-YA2	Plasma powder	95.83	4.07	0.10	–	10.0
P-YA3	(mixed with Al_2O_3 and Y_2O_3;	96.13	3.37	0.50	–	10.0
P-YA4	70%A + 30%Y)	98.14	1.76	0.10	–	10.0
P-YA5		98.77	0.23	1.00	–	10.0
P-YA6		99.28	0.22	0.50	–	15.0
A-YA1	ONODA α-SiC powder	–	–	–	–	10.0
A-YA2	(mixed with Al_2O_3 and Y_2O_3)	–	–	–	–	15.0

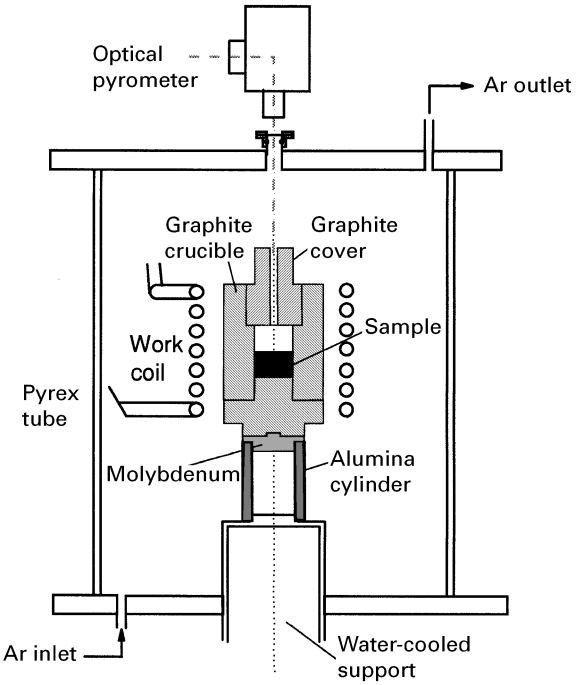

Figure 1 Schematic of the induction sintering furnace.

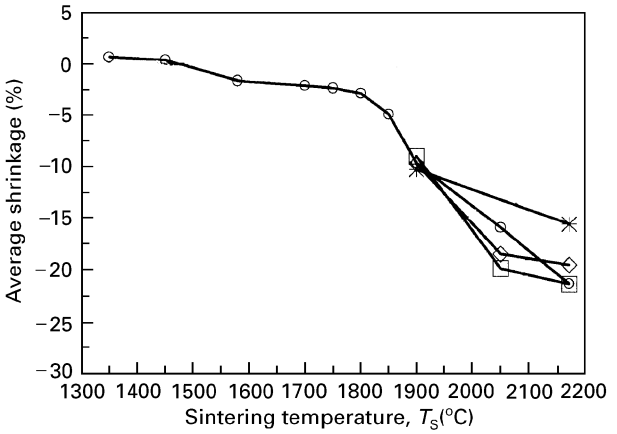

Figure 2 Linear shrinkage as a function of sintering temperature for the samples with mixed boron additions. (✳) 0.5 wt %; (○) 2.0 wt %; (□) 5.0 wt %; (◇) 10.0 wt %.

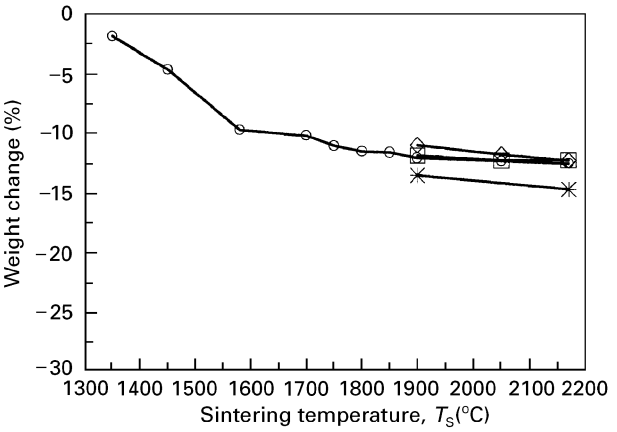

Figure 3 Weight change as a function of sintering temperature for the samples with mixed boron additions. See Fig. 2 for key.

of the starting powders and of the sintered pellets in the boron-doped series of samples. In addition, thermogravimetric analysis (TGA) in an Ar atmosphere was performed to determine adsorbed chlorides in the *in situ* B-doped powders. Fracture surfaces of the samples were examined, using scanning electron microscopy (SEM). Vicker's microhardness was performed on polished surfaces under a 1 kg load in a standard tester, with a 136° angle diamond indentor installed. X-ray diffraction analysis (XRD) was used to record phase transformation with CuK_α radiation.

4. Results using boron carbide and oxide addition as sintering aids

These were added to the synthesized powder, and the results were compared with the sintering properties of commercial powder.

4.1. Use of boron carbide (B_4C) as sintering aids

Figs 2 and 3 show the linear shrinkage and weight change as a function of sintering temperature for the various Boron (B) additions, respectively. Shrinkage and weight change in the samples with 2.0 wt % B addition were examined, beginning at a low temperature (1350 °C). It may be seen from Fig. 2 that the samples were actually expanded when fired below 1500 °C. On the other hand, significant weight losses were observed at low temperatures (4.6% at 1450 °C for instance), as may be seen in Fig. 3. This result may be related to the free carbon content and the condensed metastable SiO in the starting powders. The presence of C in the starting SiC powder was detected by XRD and TGA. A small peak of graphite was observed in the CuK_α diffraction pattern. The carbon may react with residual oxygen contained in the industrial grade argon employed, and it is thermodynamically possible that SiO reacts with free C to form SiC and CO_2 below 1600 °C. These reactions can be written as follows

$$2C(s) + O_2(g) = 2CO(g) \quad (1)$$

$$C(s) + O_2(g) = CO_2(g) \quad (2)$$

$$2SiO(g) + 3C(s) = 2SiC(s) + CO_2(g) \quad (3)$$

The produced gaseous CO and CO_2 may result in the pellet bulk expansion under the effect of their partial pressures. With the further increase of temperature, "internecking" between particles occurred, and shrinkage was visible though no densification was observed yet. For this series of powders, significant shrinkage and minor densification will not occur until temperatures above 1900 °C are reached. Under the influence of high temperatures, shrinkage and densification increased considerably, e.g. up to 21.3% at 2170 °C for shrinkage. In contrast to the shrinkage

variation trend, weight losses increased steadily with increasing temperature but reached a threshold value (9.6%) at a temperature as low as 1580 °C. Above 1580 °C weight losses increased only slightly with increasing temperature, up to 2170 °C. At high temperatures, the weight losses may be attributed mainly to reduction of residual SiO and silica layer on the surface of SiC particles

$$SiO(g) + C(s) = Si(s,l) + CO(g) \quad (4)$$

$$SiO_2(s,l) + C(s) = SiO(g) + CO(g) \quad (5)$$

$$SiO_2(s,l) + 3C(s) = SiC(s) + 2CO(g) \quad (6)$$

$$2SiO_2(s,l) + SiC(s) = 3SiO(g) + CO(g) \quad (7)$$

$$SiO_2(s,l) + 2SiC(s) = 3Si(s,l) + 2CO(g) \quad (8)$$

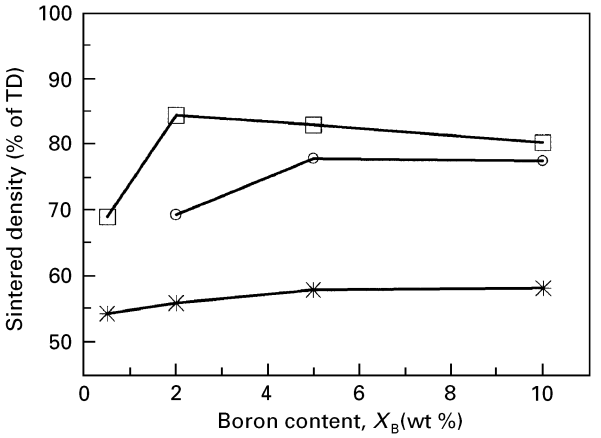

Figure 4 Effect of boron content (mixing-added) on density of SiC samples (No. P-BC1) sintered at various temperatures for 30 min. (□) 2170 °C; (○) 2050 °C; (✳) 1900 °C.

The densification of the boron-mixed powders was poor, as may be seen from Fig. 4. With the addition of 0.5 wt % B, SiC achieved a minor densification (54.3% Theoretical Density, TD) at 1900 °C. At higher temperatures, up to 2170 °C, SiC was densified to 68%. It is also seen from Fig. 4 that increasing the boron addition did not help much. At the highest temperature (2170 °C) densification decreased a little with increased boron addition. The highest density achieved was 84.5% for a 2.0 wt % B addition, sintered at 2170 °C.

As to the amount of boron addition, generally speaking, there is an obvious difference between 0.5 wt % and 2.0 wt % B additions in the shrinkage, weight loss, and densification. Among the boron additions above 2.0 wt %, the difference is difficult to be identified. Samples that were fired without major densification taking place were mainly produced as α phase polytype structures and unidimensional exaggerated grain growth also occurred at elevated temperatures. Figs 5a–d show a group of SEM fractographs of the samples with 2.0 wt % B addition fired at various temperatures for 30 min, indicating grain growth and phase transformation as function of temperature. The elongated platelike grains revealed in Fig. 5b–d are typical of α phase polytype.

4.2. Use of oxide (Al_2O_3 and Y_2O_3) as sintering aids

With the additions of oxides, the densification of SiC appeared at lower temperatures than for the case of boron addition, as may be seen in Fig. 6 for No. P-YA1 powder, where it is revealed that densification of SiC was essentially complete at the temperature of 1950 °C. The amount of added oxides seemed crucial.

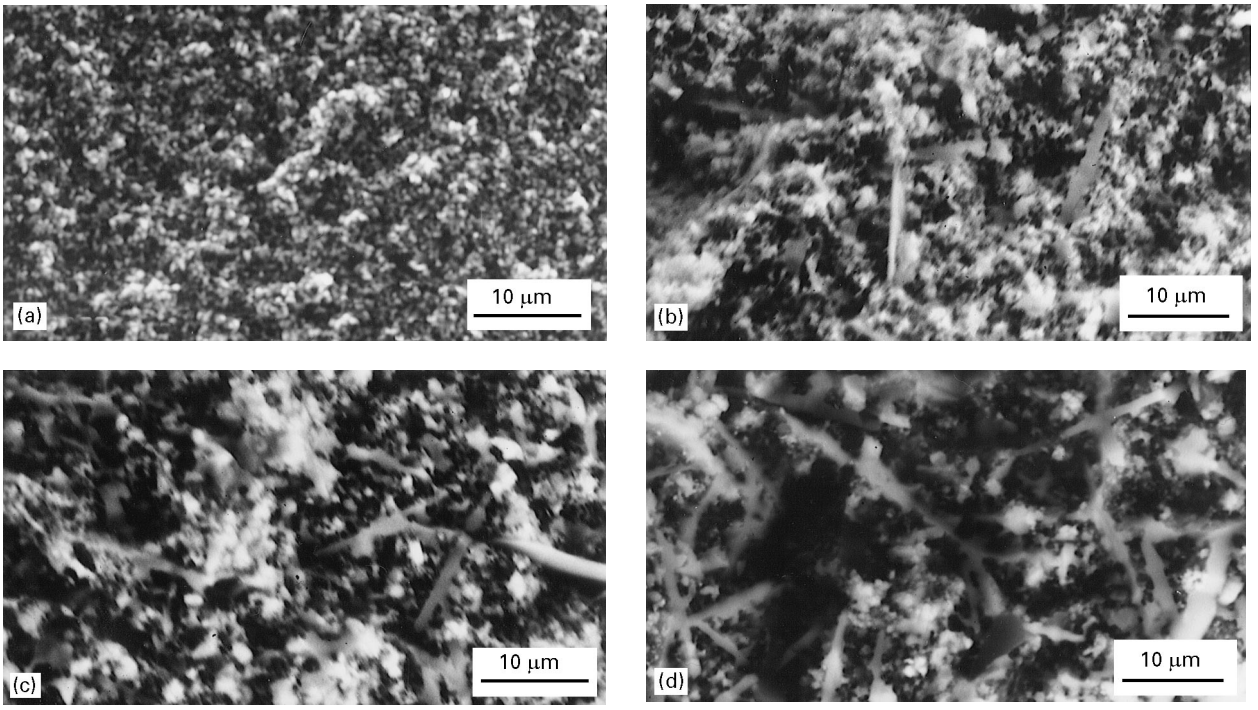

Figure 5 (a)–(d) SEM fractographs showing grain growth as a function of temperature for the samples with 2.0 wt % B addition. (a) 1900 °C; (b) 2050 °C; (c) 2100 °C (densified to 80.5%); (d) 2170 °C.

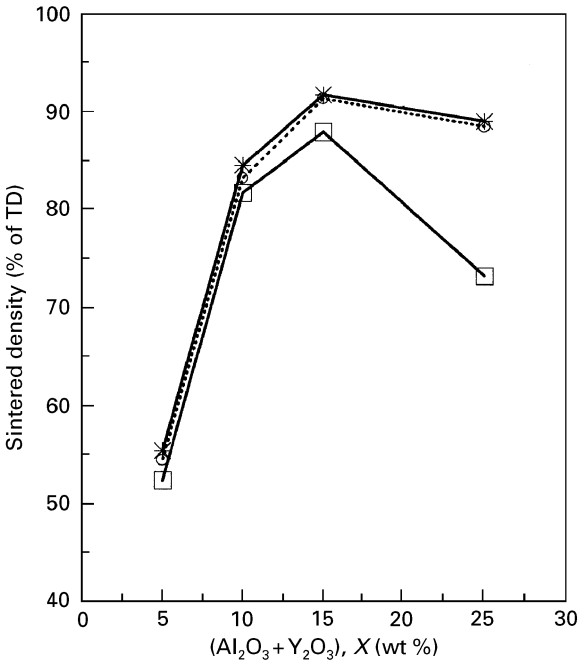

Figure 6 Effect of concentration of $(Al_2O_3 + Y_2O_3)$ (70 wt % Al_2O_3 + 30 wt % Y_2O_3) on density of SiC samples (No. P-YA1) sintered at various temperatures for 45 min. (✳) 1900 °C; (○) 1950 °C; (□) 2050 °C.

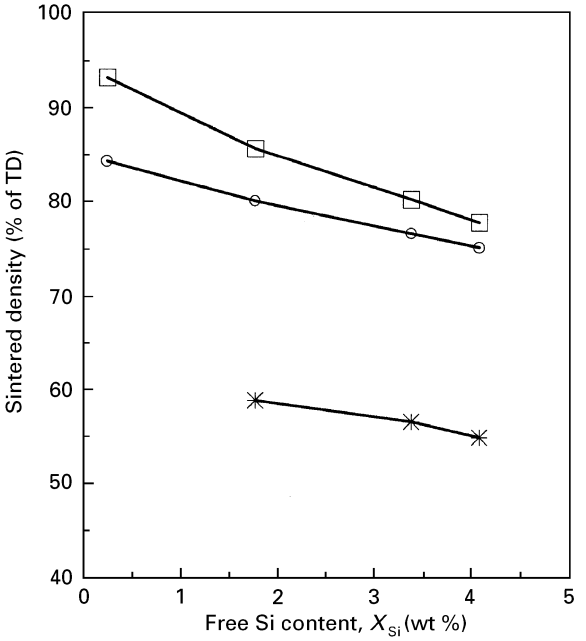

Figure 7 Effect of free Si content on density of SiC samples with 10 wt % $(Al_2O_3 + Y_2O_3)$ addition sintered at various temperatures for 45 min. (✳) 1600 °C; (○) 1800 °C; (□) 2000 °C.

It is observed that with the addition of 5 wt % (70 wt % Al_2O_3 + 30 wt % Y_2O_3), SiC powders showed only minor densification. With increasing the addition of oxides, densification increased substantially. The appropriate concentration of additive required was between 10 to 15 wt %, depending on the quality of SiC powders. Above this level, nevertheless, densification decreased.

The sintered density of SiC is normally considerably affected by impurities in the starting powders, as is the condition for same amount of dopants. Thus it was demonstrated that the sintered densities decreased with increasing free Si contents in the powders at different temperatures, as shown in Fig. 7. For instance, at 2000 °C for 45 min, the sintered density for the powder containing 0.23 wt % free Si was 93.3%, whereas the sintered density for the powder containing 4.07 wt % free Si was only 77.9%. It is also shown that the densification of the powder containing the lower free Si was more sensitive to temperature increase than for the powder containing the higher free Si. For those samples with high free Si impurities densification was nearly complete at around 1800 °C, and with further increasing temperature, the densification increased slightly, but grain growth increased substantially.

Densification of SiC powders with oxide additions is also a function of the sintering time. It is found that the sintered densities reached the maximum after 75 min soaking, and it seems that at low temperature (1800 °C) soaking time has a significant influence on the densification, but at high temperature (2000 °C) the influence of soaking time on the densification is less significant. In the latter case, 15 min holding at sintering temperature would be sufficient for attaining the highest density. It may be seen from Fig. 8 that at both temperatures (1800 and 2000 °C) the sintered densities decreased as the soaking time was extended to 120 min. The reason for this may also be related to grain growth. It is thought that the use of UFP may lower sintering temperature and meanwhile shorten sintering time, since the beneficial role of large specific surface of UFP no longer exists as the sintering time is extensively prolonged.

With improvement of the purities of the synthesized SiC powders, sintered density of the sample with the addition of 10 wt % (70 wt % Al_2O_3 + 30 wt % Y_2O_3) may be up to 95% of theoretical at 2000 °C for 75 min, as shown in Fig. 9 for P-YA5 powder, where the results for commercial α-SiC powder are also indicated for the comparison purposes. The sintering of commercial β-SiC powder (Ibiden Betarundum) was also tested but was not successful, due to the difficulty in preparation of green pellets (serious layering phenomenon). It is revealed from Fig. 9 that the sintered density of the plasma synthesized SiC UFP with the 10 wt % $(Al_2O_3 + Y_2O_3)$ addition (95% of TD at 2000 °C for 75 min) is higher than that for the commercial SiC (less than 90%) sintered under the same conditions, although the latter had a higher green density (56–59% of TD), implying that the plasma produced powders are easier to sinter than the commercial powders. On the other hand, with 15 wt % $(Al_2O_3 + Y_2O_3)$ addition, the plasma-synthesized powder achieved final densification at a temperature as low as 1800 °C, whereas the commercial powder still required a high temperature of up to 2000 °C. Figs 10 and 11 show the shrinkage and weight change corresponding to the samples shown in Fig. 9, respectively. It may be seen that for both types of powders, the shrinkage increased with increasing

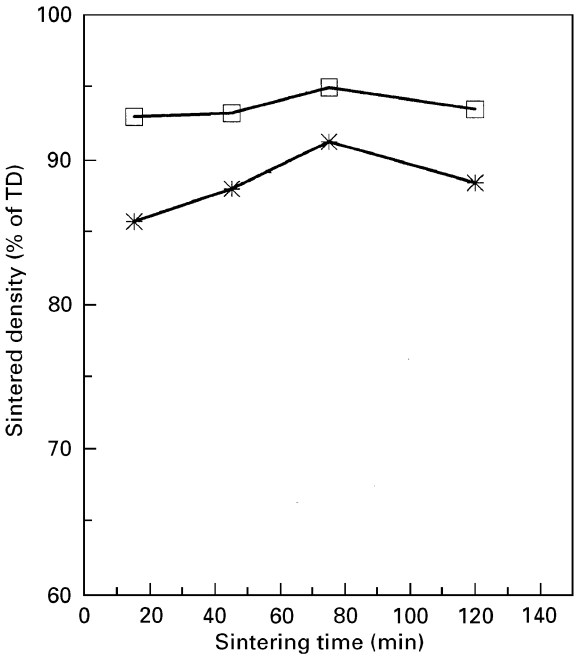

Figure 8 Effect of firing time on density of various SiC samples with 10 wt % ($Al_2O_3 + Y_2O_3$) addition sintered at various temperatures. (✳) 1800 °C; (□) 2000 °C.

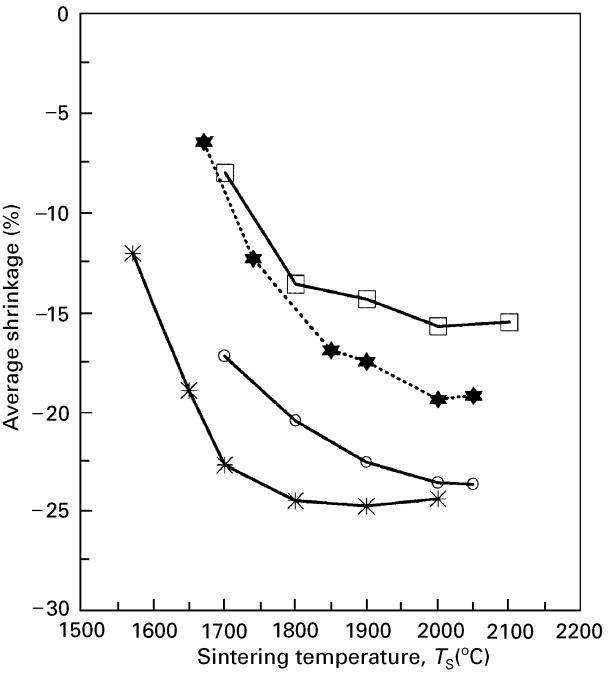

Figure 10 Linear shrinkage as a function of sintering temperature for the samples with oxide additions. See Fig. 9 for key.

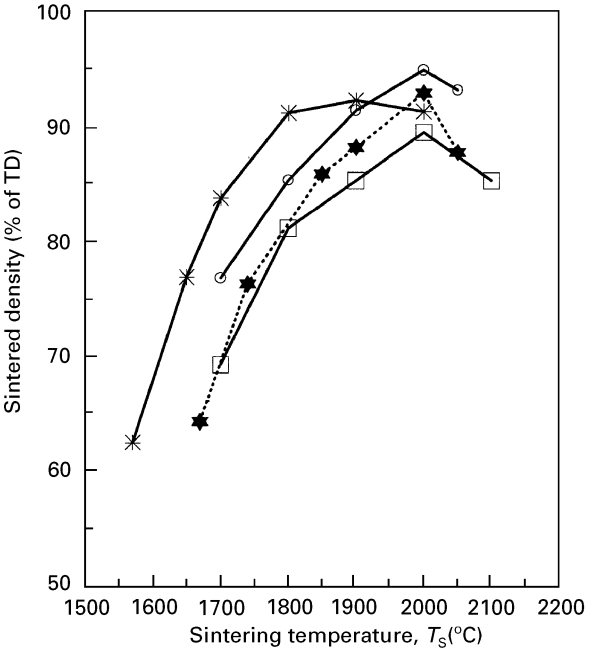

Figure 9 Effect of temperature on density of various SiC samples sintered for 75 min. (○) Plasma-SiC + 10 wt % AY; (✳) Plasma-SiC + 15 wt % AY; (□) Onoda-SiC + 10 wt % AY; (★) Onoda-SiC + 15 wt % AY.

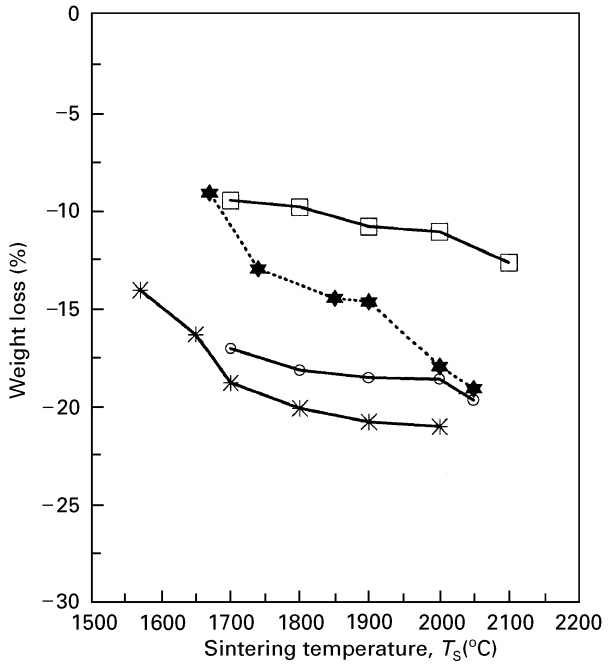

Figure 11 Weight change as a function of sintering temperature for the samples with oxide additions. See Fig. 9 for key.

temperature until a plateau value was attained, whereas the weight loss continuously increased with increasing temperature. It is obvious that the plasma powder had higher shrinkage and weight loss than the commercial powder, and with increasing oxide additions, both shrinkage and weight loss were increased. In the case of the oxide additions, the existing volatile components of CO, CO_2, and SiO, as already discussed previously, are joined by a new component, Al_2O. It would be generated from the introduced Al_2O_3 through the following reaction

$$SiC + Al_2O_3 = SiO + CO + Al_2O \quad (9)$$

This gave rise to the result that the weight losses experienced with the oxide additions were generally higher than those with boron addition, but not necessarily proportional to the actual generation of Al_2O because of the varying starting powder compositions.

TABLE II Vicker's microhardness measurements for the sintered compacts[a]

Sample No.	H_V (GPa)
P-YA5	31.2 ± 2.2
P-YA6	29.3 ± 2.8
A-YA1	27.4 ± 2.0
A-YA2	28.2 ± 3.2

[a] Average for 15 measurements on the polished surface.

The Vicker's microhardness measurements for both types of sintered compacts, listed in Table II, show that the hardness value for the sintered pellet from plasma powder with 10 wt % ($Al_2O_3 + Y_2O_3$) addition (No. P-YA5) reached 31.2 GPa, whereas it is 27.4 GPa for the sintered pellet from commercial α-SiC powder (No. A-YA1). At a higher percentage of ($Al_2O_3 + Y_2O_3$) addition (15 wt %), the sintered pellet from the plasma powder also had a higher hardness value than that from commercial powder.

Fig. 12 shows the fractographs of the sintered pellets for Nos. P-YA5 and A-YA1. It may be observed that the microstructure of No. P-YA5 is uniform and fine-grained; the grain size is in the range 0.1 to 0.5 μm, while the grain size for No. A-YA1 is 1 to 3 μm.

It is widely accepted that the sintering of SiC with oxide additives is based on a liquid phase sintering mechanism. Thermodynamic investigations indicate that a liquid phase can form at the sintering temperatures by the reaction of SiC with Al_2O_3 [30] and a liquid can form among SiC, Al_2O_3 and Y_2O_3 [25] at temperatures as low as 1700 to 1800 °C. Prior studies [24, 25, 31] showed that 10 wt % ($Al_2O_3 + Y_2O_3$) addition is generally necessary for sintering of Si_3N_4 and SiC to high density, which is consistent with the present results.

5. Results of *in situ* boron doping of the powder in the synthesis step

5.1. Analysis of the boron-doped SiC powders

The SiC UFP with *in situ* boron-doping was synthesized under the similar plasma operation conditions to those for undoped powders. They had similar compositions to those for undoped powders, except for the introduction of chlorides, as detected by EPMA. Figs 13a and b show energy dispersive spectroscopy (EDS) patterns for undoped (No. PH-B0) and boron-doped SiC UFP (No. PH-B2), respectively. It may be seen from Fig. 13b that the K_α line for Cl is apparent for No. PH-B2. This means that the B-doped powder contains some adsorbed, unreacted BCl_x and/or HCl. Using PGNAA, it is determined that boron content in No. PH-B2 powder was 1.65 wt %. By means of XPS detection technique, it is possible to identify the forms of boron existing in the powder (a surface depth of a few nanometres). A V.G. Scientific XPS analyser was used for this purpose. The X-rays used to bombard the sample were monochromatic MgK_α rays with an energy of 1253.6 eV. Two different powder mounting methods (i.e. indium foil and adhesive tape methods) were compared and no significant difference was observed in terms of the XPS peaks and their positions. The indium foil method was used here. Experiments showed that static charging of the sample could result in an increase of 0.4–2.3 eV in the peak position compared with standard data. The carbon 1s peak, arising from traces of hydrocarbons in the spectrometer and from free carbon contained in the powder, was used as a reference for evaluating the peak positions. The C_{1s} peak shift due to charging was taken as the average value minus the value of 284.6 eV, obtained from standard data [32]. Fig. 14 shows the corrected XPS patterns of B_{1s} for the B-doped UFP samples. Three forms of boron are detectable in Nos. PH-B2 and PH-B3 samples, at binding energy level of ~191 eV, ~193 eV, and ~200 eV, respectively. Based on the law of Binding energy (BE) shifts [33], we assign them to BN, B_2O_3, and BCl_x residue, respectively. Metallic B was also detectable, not shown here, in other samples with different B-dopings.

The formation of BN was not so surprising, considering that the SiC powders were synthesized in an $Ar + N_2$ plasma gas mixture. The reaction, $2B + N_2 = 2BN$, is thermodynamically feasible [34]. In addition, the undetectability of B_4C can also be explained from the viewpoint of thermodynamics. In a nitrogen

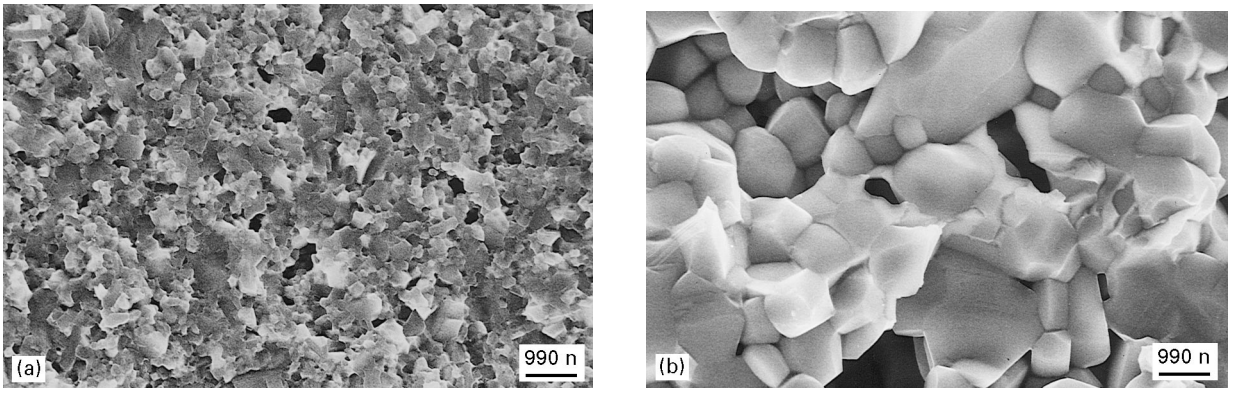

Figure 12 SEM fractographs of various SiC samples with 10 wt % ($Al_2O_3 + Y_2O_3$) sintered at 2000 °C for 75 min, (a) from plasma powder (No. P-YA5) and (b) from Onoda α-SiC powder (No. A-YA1).

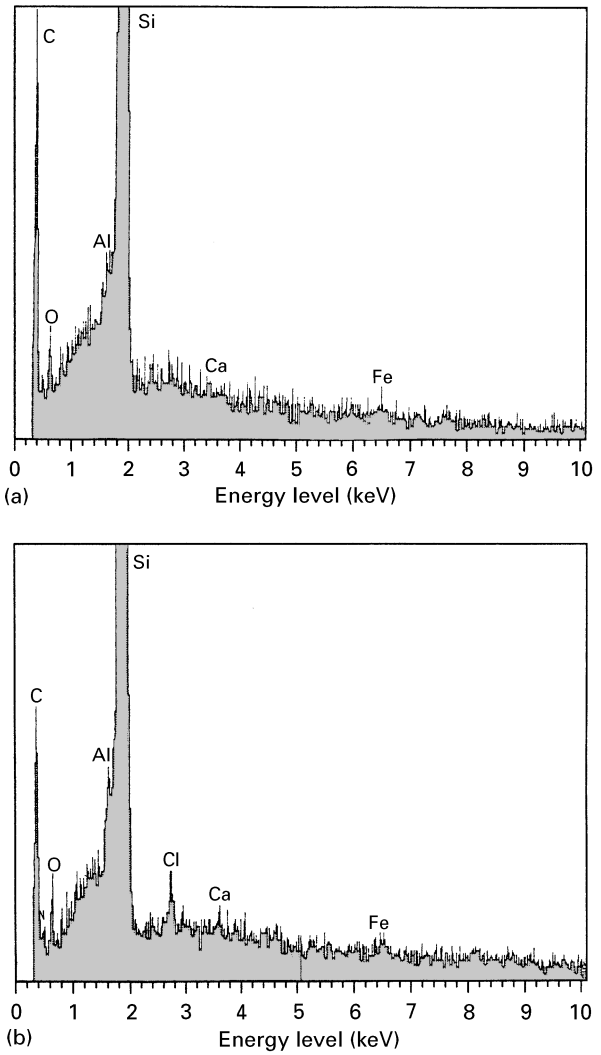

Figure 13 EDS patterns for the undoped and boron-doped plasma powders. (a) undoped (No. PH-B0) and (b) *in situ* B-doped (1.65 wt % B) (No. PH-B2).

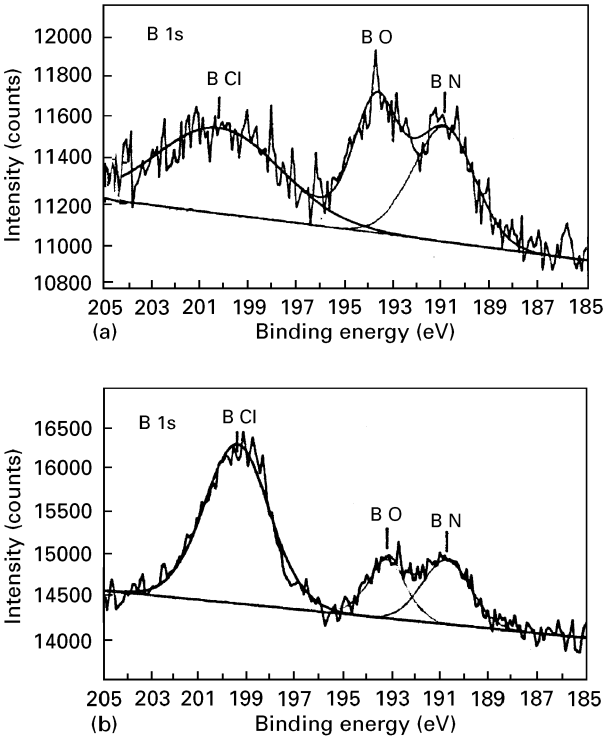

Figure 14 XPS spectra of B_{1s} for boron-doped powders, showing the forms of boron existing in the doped powders. (a) No. PH-B2 powder and (b) No. PH-B3 powder.

TABLE III Thermogravimetric analysis for the boron-doped SiC powders

Sample No.	Boron content (wt %)	Weight loss (%)	Occurring temperature (°C)
PH-B0	0	0	240
PH-B1	0.63	1.5	270
PH-B2	1.65	3.0	240
PH-B3	3.90	4.0	240

atmosphere, the performed boron carbide can be converted to boron nitride according to the following reaction

$$\tfrac{1}{2}B_4C + N_2 = 2BN + \tfrac{1}{2}C \qquad \Delta G_T^0 \ll 0 \qquad (10)$$

B_2O_3 is easily formed when boron is exposed to oxygen partial pressure, and it is highly hygroscopic. It also has a very low melting point (variously reported as 723 K [34] or >773 K [35]. The occurrence of the B–Cl peak in the B_{1s} spectra shown in Fig. 14a and b is apparently caused by unreacted boron source material, and this was confirmed by thermogravimetric analysis (TGA). A heat treatment (up to 1000 °C) of the boron-doped powders in an Ar atmosphere was done using TGA, and the results are shown in Table III. It is indicated that as the boron content in the powders increases, weight loss increases also. It is noted that the maximum weight loss occurred in the temperature range of 240 to 280 °C, which is thought to be caused by the desorption of HCl and unreacted BCl_x. As the atomic weight ratio, B : Cl, in BCl_3 is up to 1 : 10, the introduction of large amount of Cl accompanying boron doping is inevitable.

5.2. Densification of the boron-doped powders

Fig. 15 shows the densification of the B-doped powders as a function of sintering temperature. It may be seen that minor densification occurred at temperatures as low as 1880 °C, and at 2100 °C, the powders are able to be densified to 90% of theoretical with 1.65 wt % boron doping At low boron content (0.63 wt %), the density achieved was 75% TD under the sintering conditions of 2000 °C and 30 min, and it did not increase further with increased temperature due to the offset of rapid grain growth. However, it is observed that at high boron contents ($\geqslant 1.65$ wt %), densification increased significantly with increasing temperature.

Fig. 15 also shows that densification decreases after boron doping has reached a certain value

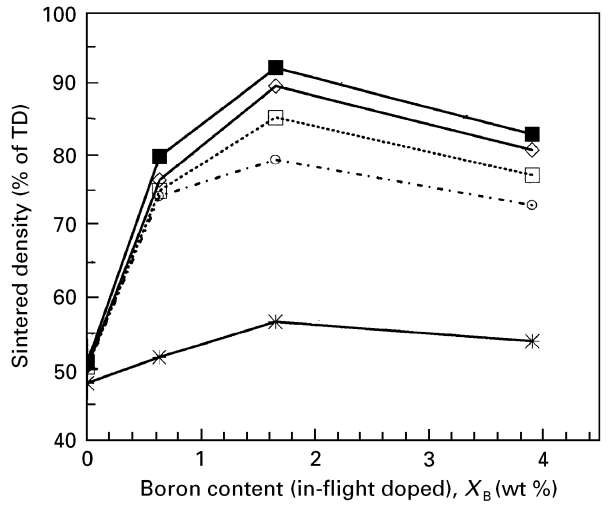

Figure 15 Effect of boron content (*in situ* doped) on density of SiC samples sintered at various temperatures for 30 min. (■) 2050 °C; ϕ4 mm; (◇) 2100 °C; (□) 2050 °C, ϕ1.5 mm; (○) 2000 °C; (✳) 1880 °C.

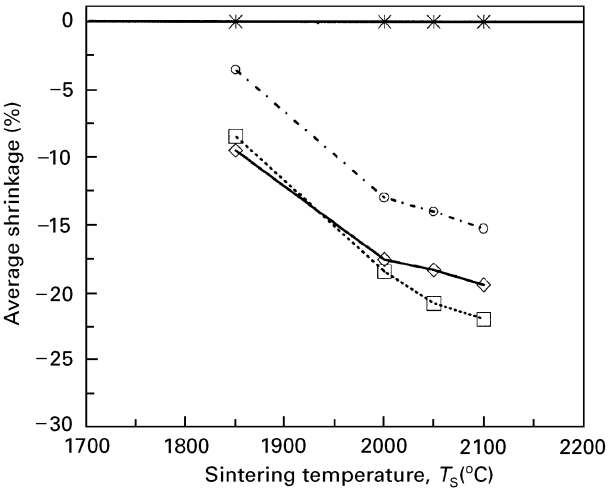

Figure 16 Linear shrinkage as a function of sintering temperature for the samples with *in situ* doped boron. (✳) 0; (○) 0.63 wt %; (◇) 3.9 wt %; (□) 1.65 wt %.

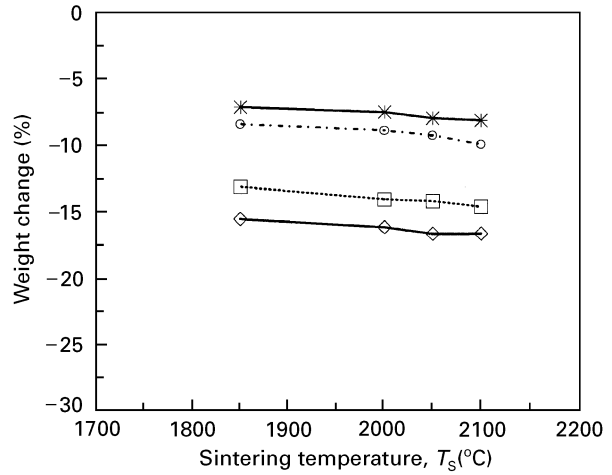

Figure 17 Weight change as a function of sintering temperature for the samples with *in situ* doped boron. (✳) 0; (○) 0.63 wt %; (◇) 3.9 wt %; (□) 1.65 wt %.

(1.65 wt % in the present case). This phenomenon may be explained from the viewpoint of both the boron solubility limit in SiC and chloride contamination in the powders, with increased boron doping, the latter being a problem arising from the boron source material employed, as mentioned above. Figs 16 and 17 show the shrinkage and weight change as functions of temperature for the SiC powders with various boron dopings, respectively, which corresponds to the case in Fig. 15. It may be seen from Fig. 16 that no shrinkage was observed for the undoped powder at all temperatures. With 0.63 wt % B doping, however, shrinkage occurred at the temperature of 1880 °C, and increased considerably with increasing temperatures up to 2100 °C. The influence of boron doping on the shrinkage was also significant if comparing the case of 0.63 wt % B with that of 1.65 wt % B. However, there is no shrinkage improvement observed when increasing B-doping from 1.65 to 3.90 wt %; by contrast, at high temperatures the shrinkages with 3.90 wt % B were less than those for 1.65 wt % B. This variation trend is partially due to the introduction of excessive chlorides in the powder with the high boron doping during synthesis. The weight change shown in Fig. 17 is in a similar relationship to that already described previously for the case of boron admixing, i.e. weight loss reached a high level at relatively low temperature and increased only slightly with increasing temperature up to 2100 °C. It is noted from Fig. 17 that the undoped powders lost weight by some 7 to 8% during firing even though no shrinkage was observed. This weight loss mechanism is the same as that discussed before for the B-admixed powder, specifically being due to the Reactions 1, 2 and 3. With 0.63 wt % B doping, the weight losses increased to 8.3 to 9.8% at different temperatures. The 1.3 to 1.8% extra weight loss (compared to the undoped case) is in approximate agreement with the adsorbed chlorides determined by TGA analysis shown in Table III, being attributed to the absorbed HCl and BCl_x, which desorbed below 300 °C. With B-doping increased from 0.63 wt % to 1.65 wt % and to 3.90 wt %, the weight losses increased substantially, far beyond the values of 3 and 4% indicated in Table III, for No. PH-B2 and No. PH-B3, respectively. This suggests that there are some other sources which also contributed to the weight loss besides the HCl and BCl_x mentioned above. One of the most probable sources is B_2O_3, which formed with the injection of BCl_3 into the reaction system during plasma powder synthesis step. XPS has already confirmed the presence of B_2O_3 in the doped powders (see Fig. 14). XPS for the sintered pellets, on the other hand, indicated that the peak characteristic of B–O bonding in the XPS pattern do disappeared after sintering, as may be seen in Figs 18a and b. Comparing Fig. 18 with Fig. 14, the absence of B–O bonding after sintering is obviously revealed. Liquid B_2O_3 has quite a high vapour pressure. In addition, under sintering temperatures (>1800 °C) the following reactions are

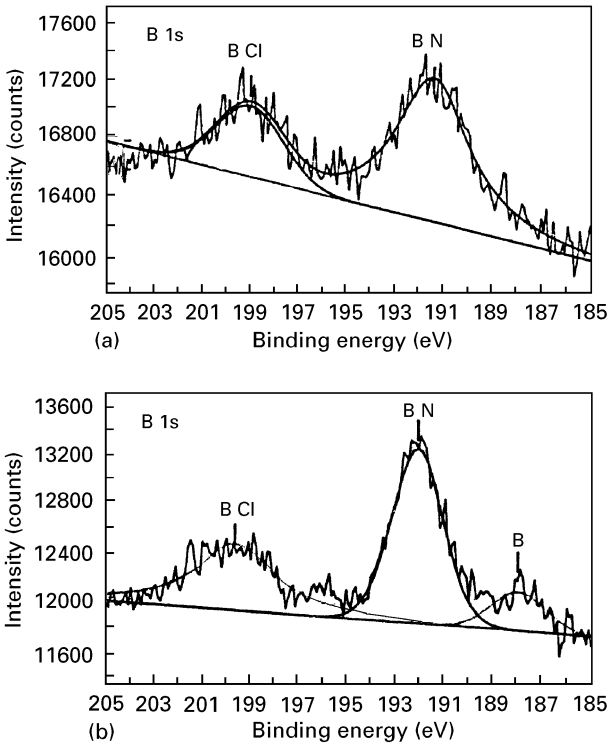

Figure 18 XPS spectra of B_{1s} for sintered pellets, showing the disappearance of boron oxide peak after sintering. (a) No. PH-B2 pellet and (b) No. PH-B3 pellet.

thermodynamically feasible

$$2B_2O_3(s,l) + 7C(s) = B_4C\ (s) + 6CO(g) \quad (11)$$

$$B_2O_3(s,l) + 3C(s) = 2B(s) + 3CO(g) \quad (12)$$

This may explain why B_2O_3 partially contributed to the weight loss that occurred during the sintering of the B-doped SiC powders. If we make a comparison between Fig. 3 and Fig. 17, it can be found that generally the weight loss for B-doped powder is 2–3% higher than for the B-admixed powder. If the chloride contamination is taken into consideration, the total weight changes for the two cases are actually equivalent. The difference lies in that for the B-admixed powder weight loss arised from free carbon and silicon oxide, whereas for the B-doped powder part of the silicon oxide was replaced by boron oxide. Browning *et al.* [36] has previously observed the association of B-rich particles with oxide in commercial pressureless sintered α-SiC; B and C being used as sintering aids. They attributed the majority of the oxygen-rich areas found in much product to the residual oxide films typically found on submicron SiC powder particles or by partial oxidation of B-rich phases during sintering in gases (e.g. Ar or N_2) of commercial purity, i.e. the boron oxide seems unavoidable.

It is of interest to note that densification of the boron-doped powders was improved with the use of a graphite cover having a larger hole (ϕ4 mm) in the centre, compared to the case of ϕ1.5 mm, as shown in Fig. 15. At the level of 0.63 wt % B doping, densification of the powders made no apparent difference. At higher dopings (1.65 and 3.90 wt % B), however, the difference in relative density may be of the order of 7%. While the reason for this is open to argument, one probable explanation is that the larger opening in the crucible top allowed easier escape for the gaseous species generated during sintering, particularly any HCl and unreacted BCl_x adsorbed and/or trapped in the starting powders. It was observed that there were some condensates deposited on the inner wall of the cover hole after sintering, and these condensates nearly blocked the hole in the case of 1.5 mm diameter. It may be inferred that during sintering the generated gaseous species would not escape promptly but stagnated and accumulated on the top of the specimens, forming a thick vapour layer comprising HCl, BCl_x, CO, CO_2, SiO and B_2O_3, and this unusual atmosphere would be detrimental for the densification of SiC compacts. Through the use of a large hole cover, the escape of gaseous volatiles was substantially facilitated. The result presented here implies that if a large amounts of volatile components are being generated during sintering these components should be able to escape from the system as quickly as possible.

Fig. 19 shows the EDS pattern produced for the fractured surface of the sintered pellet No. PH-B2, demonstrating the absence of chlorine and decreased oxygen level after sintering, compared with the unsintered boron-doped powder (Fig. 13b). This also lends confirmation to the generation of gaseous species during sintering process. In spite of the absence of chlorine in EDS pattern, B–Cl bonding is still visible in the B_{1s} XPS pattern (Fig. 18). This may be attributed to chloride condensates on the specimen surface after firing, considering the great sensitivity of XPS for chlorine.

The findings mentioned above suggest that an appropriate post-production treatment is required for the *in situ* B-doped UFP to remove adsorbed chlorides before sintering.

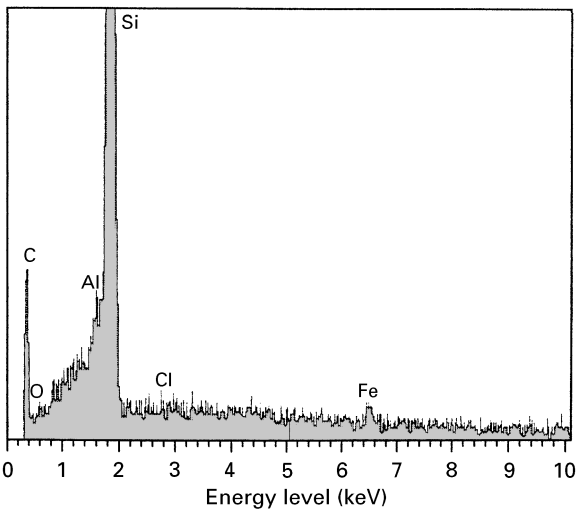

Figure 19 EDS pattern for SiC sample (No. PH-B2) sintered at 2050 °C for 30 min, showing the disappearance of Cl peak and decreased oxygen level after sintering.

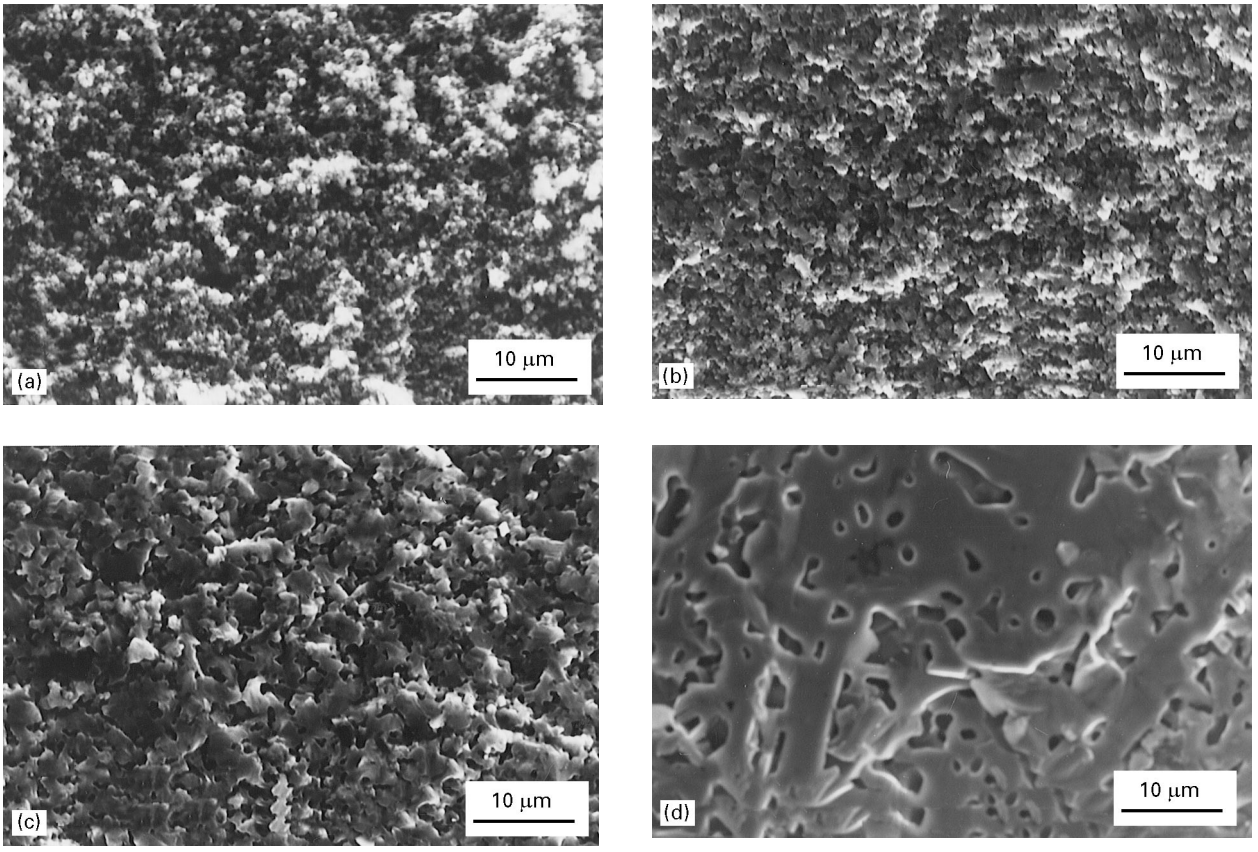

Figure 20 SEM fractographs of SiC sample (No. PH-B2) with 1.65 wt % B sintered at various temperatures for 30 min. (a) 1880 °C; (b) 2000 °C; (c) 2050 °C, and (d) 2100 °C.

5.3. Comparison of *in situ* B-doping with B-admixing

The advantages of boron *in situ* doping over admixing were revealed by the following observations. Firstly, the *in situ* boron-doped plasma powder, with 1.65 wt % B, was densified to 85.32% at 2050 °C for 30 min, which is more than 100 °C lower than the sintering temperature required for the 2.0 wt % boron-mixed powder, which fired to almost the same density. Under the same sintering conditions, the boron-mixed powder was densified to only 69%, as it may be seen in Fig. 4. With *in situ* boron doping of 0.63 wt %, at the temperature of 2000 °C SiC powder densified to 75%, as mentioned above, which is 6% higher than the highest density achieved for the 0.5 wt % B-mixed powders, but at a temperature more than 100 °C lower. Secondly, the microstructure of the sintered parts produced with *in situ* boron-doped powders is uniform and fine-grained. Grain sizes are less than 5 μm as may be seen in Fig. 20 which displays the fractographs of No. PH-B2 sintered at different temperatures. Occasional, elongated grains (up to 30 μm) were observed only for the sample sintered at 2100 °C, as revealed in Fig. 20d.

The improvement in sinterability for the in-flight B-doped powders arose from the micro-dispersion of the dopant in SiC particles during the plasma synthesis step and thus a homogeneous mixing of dopant and matrix material, whereas it is nearly impossible to attain such a homogeneous mixing in the case of SiC powder with separate B_4C. The inhomogeneity of mixing may give rise to microcracks in the SiC sample during sintering, the result of differential shrinkage in heterogeneous compositions.

6. Summary and conclusions

In spite of the beneficial results achieved with the plasma-synthesized UFP, sintered densities were still not as high as expected, an outcome that may be attributed to the following circumstances. First of all, the sintering conditions were not optimized in the present study, investigation of which would be a long task. A very fast heating rate was generally adopted in the sintering tests, which facilitated the control of the sintering conditions for the various powders. Unfortunately, however, this may encourage cracks and entrapment of volatile components in the compact, resulting in porosity. Secondly, the green densities achieved were relatively low, at only around 47–50%. This is a problem that is often encountered in the handling of UFP, probably due to its very narrow particle size distribution and/or formation of agglomerates. It is well known that the high green density is very important for optimum densification. Thus Futaki *et al.* [31] had to convert amorphous Si_3N_4 UFP (average particle size 0.03 μm) to partially

crystallized Si_3N_4 powder (0.2 μm) to increase the green density of compacts. Thirdly, SiC UFP contains various impurities such as oxygen, chlorides, free Si, free C and metallic elements originating from the source materials. The *in situ* B-doped SiC powders generally displayed considerable sintering shrinkage (up to 23.5% for No. PH-B2 sintered at 2050 °C for 30 min, using a large hole cover). However, the weight loss was also substantial (up to 14.8%), which was caused by the generation of gaseous species during sintering, including B_2O_3, CO, CO_2, SiO, etc., as well as the desorption of HCl and/or unreacted BCl and BCl_3. The generation of the large volumes of volatilization components leads to difficulty in further pore removal and density maximization.

Based on the present experimental study, we can draw the following conclusions:

1. SiC UFP synthesized from elemental Si and CH_4 using induction plasma was pressureless sintered to 95% of theoretical at 2000 °C for 75 min with the addition of 7 wt % Al_2O_3 + 3 wt % Y_2O_3. The Vicker's microhardness value was up to 31.2 GPa. These values are superior to those for the commercial α-SiC powder sintered under the same conditions.
2. Pressureless sintering of the plasma-synthesized SiC powder with the addition of B_4C was partially densified with the highest density of 84.5% being achieved at 2170 °C for 30 min. However, the *in situ* boron-doped powder during plasma synthesis is able to be densified to 92% at 2050 °C for 30 min, mainly due to the very homogeneous mixing of B with SiC.
3. The plasma-synthesized powders displayed large shrinkage and on the other hand substantial weight loss during sintering, which was caused by the generation of a number of gaseous species, such as CO, CO_2, SiO, Al_2O, B_2O_3, HCl and BCl_x. Vaporization is detrimental to densification.
4. High density, near theoretical, may be achieved under the present sintering conditions with the use of high purity starting powders. Such powders can be synthesized by using high-purity elemental Si source material and strictly controlled reaction atmosphere in plasma. These powders should be handled in an oxygen-free atmosphere. Post-production treatment is required for the *in situ* B-doped powders to remove the adsorbed chloride contaminants.

Acknowledgements

The authors gratefully acknowledge the financial support of the Conseil de Recherche en Sciences Naturelles et en Génie du Canada (CRSNG) and the Fonds pour la Formmation de Chercheurs et l'Aide a la Recherche (FCAR). Dr Alice Pidruczny at McMaster University undertook the prompt gamma neutron activation analysis. We also appreciate Dr Peter Lanigan's contribution for his effort in the proofreading of this paper.

References

1. C. M. HOLLABAUGH, D. E. HULL, L. R. NEWKIRK and J. J. PETROVIC, *J. Mater. Sci.* **18** (1983) 3190.
2. G. J. VOGT, R. S. VIGIL, L. R. NEWKIRK and M. TRKULA, in Proceedings of 7th International Symposium on Plasma Chemistry, Eindhoven, Netherlands, July 1985.
3. A. MITSUI and A. KATO, *Yogyo Kyokaishi (Japan)* **94** (1986) 517.
4. H. R. BAUMGARTNER and B. R. ROSSING, "Pressureless sintering and properties of plasma-synthesized SiC powder, Ceramic transactions, Vol. 2: Silicon Carbide '87, edited by J. D. Cawley and C. E. Semler (American Ceramics Society, Westerville, OH, 1989) p. 3.
5. T. KAMEYAMA, K. SAKANAKA, A. MOTOE, T. TSUNODA, T. NAKANAGA, N. I. WAKAYAMA, H. TAKEO and K. FUKUDA, *J. Mater. Sci.* **25** (1990) 1058.
6. P. R. TAYLOR and S. A. PIRZADA, *Mater. Manuf. Proc.* **8** (1993) 501.
7. R. M. SALINGER, *Ind. Eng. Chem. Prod. Res. Develop.* **11** (1972) 230.
8. J. Y. GUO and G. L. ZHENG, *Engng Chem. Metall. (China)* **12** (1991) 1.
9. C. W. ZHU, G. Y. ZHAO, V. REVANKAR and V. HLAVACEK, *J. Mater. Sci.* **28** (1993) 659.
10. M. ENDO, T. SANO, N. URASATO and M. SHIRAISHI, *Yogyo-Kyokai-Shi (Japan)* **95** (1987) 104.
11. P. C. KONG, T. T. HUANG and E. PFENDER, in Proceedings of 6th International Symposium on Plasma Chemistry, Montreal, Canada, July 1983, A-7-2.
12. P. KONG, R. M. YOUNG, T. T. HUANG and E. PFENDER, in Proceedings of 7th International Symposium on Plasma Chemistry, Eindhoven, Netherlands, July 1985, B-4-4.
13. J. Y. GUO, F. GITZHOFER and M. I. BOULOS, *J. Mater. Sci.* **30** (1995) 5589.
14. S. PROCHAZKA, in Proceedings of the Conference on Ceramics for High Performance Applications, edited by J. J. Burke *et al.* (1973) p. 239.
15. J. A. COPPOLA, L. N. HAILEY and C. H. MCMURTY, US Patent, No. 4, 124,667, Nov. 7 (1978).
16. J. E. LANE, C. H. CARTER and R. F. DAVIS, *J. Amer. Ceram. Soc.* **71** (1988) 281.
17. R. H. J. HANNINK, Y. BANDO, H. TANAKA and Y. INOMATA, *J. Mater. Sci.* **23** (1988) 2093.
18. R. M. WILLIAMS, B. N. JUTERBOCK, S. S. SHINOZAKI, C. R. PETERS and T. J. WHALEN, *Amer. Ceram. Soc. Bull.* **64** (1985) 1385.
19. W. BOCKER, H. LANDFERMANN and H. HAUSNER, *Powder Metall. Int.* **10** (1978) 87.
20. K. A. SCHWETZ and A. LIPP, *Sci. Ceram.* **10** (1980) 149.
21. D. H. STUTZ, S. PROCHAZKA and J. LORENZ, *J. Amer. Ceram. Soc.* **68** (1985) 479.
22. S. SHINOZAKI, R. M. WILLIAMS, B. N. JUTERBOCK, W. T. DORLON, J. HANGAS and C. R. PETERS, *Amer. Ceram. Soc. Bull.* **64** (1985) 1389.
23. M. OMORI and H. TAKEI, *J. Amer. Ceram. Soc.* **65** (1982) C-92.
24. M. A. MULLA and V. D. KRSTIC, *Ceram. Bull.* **70** (1991) 439.
25. S. K. LEE and C. H. KIM, *J. Amer. Ceram. Soc.* **77** (1994) 1655.
26. J. KONDO and G. SAIKI, *Ceram. Trans. 1A, Amer. Ceram. Soc.* (1988) 285.
27. T. J. CARBONE and B. R. ROSSING, in Proceedings of 2nd International Symposium on Ceramic Materials and Components for Engines, West Germany, April 14–17 (1986).
28. O. CROIX, M. GOUNOT, P. BERGEZ, M. LUCE and M. CAUCHETIER, Paper presented at the 7th Cimtec, Montecatini, Terme, Italy, June 24–30 (1990).
29. K. M. RIGTRUP and R. A. CUTLER, in "Ceramic transaction," Vol. 2. Silicon Carbide '87, edited by J. D. Cawley and C. E. Semler (American Ceramics Society, Westerville, OH, 1989) p. 17.
30. A. K. MISRA, *J. Amer. Ceram. Soc.* **74** (1991) 345.

31. S. FUTAKI, Y. SHIMIZU, K. SHIRAISHI, Y. MORIYOSHI, T. SATO and T. SAKAI, *J. Mater. Sci.* **22** (1987) 4331.
32. C. D. WAGNER, W. M. RIGGS, L. E. DAVIS, J. F. MOULDER and G. E. MUILENBERG (eds), "Handbook of X-ray photoelectron spectroscopy" (Perkin-Elmer Corp., 1978).
33. A. W. CZANDERNA (ed.), "Methods of surface analysis" (Elsevier Scientific Publishing Company, Amsterdam, 1975).
34. "JANAF Thermochemistry Tables", *J. Phys. Chem. Ref. Data.* **14** (1985) Suppl. 1.
35. M. J. AZIZ, E. NYGREN, J. F. HAYS and D. TURNBULL, *J. Appl. Phys.* **57** (1985) 2233.
36. R. BROWNING, J. L. SMIALEK and N. S. JACOBSON, *Adv. Ceram. Mater.* **2** (1987) 773.

Received 20 November 1995
and accepted 3 February 1997